


The Impact of Land-Surface Parameter Properties and Resolution on the Simulated Cloud-Topped Atmospheric Boundary Layer

Leonhard Gantner¹  · Vera Maurer^{1,2} ·
Norbert Kalthoff¹ · Olga Kiseleva¹

Received: 15 June 2016 / Accepted: 18 July 2017 / Published online: 17 August 2017
© Springer Science+Business Media B.V. 2017

Abstract Sensitivity tests using the ‘Consortium for Small Scale Modeling’ model in large-eddy simulation mode with a grid spacing of 100 m are performed to investigate the impact of the resolution of soil- and vegetation-related parameters on a cloud-topped boundary layer in a real-data environment. The reference simulation uses the highest land-surface parameter resolution available for operational purposes (300 m). The sensitivity experiments were conducted using spatial averaging of about $2.5 \text{ km} \times 2.5 \text{ km}$ and $10 \text{ km} \times 10 \text{ km}$ for the land-surface parameters and a completely homogeneous distribution for the whole model domain of about $70 \text{ km} \times 70 \text{ km}$. Additionally, one experiment with a higher mean soil moisture and another with six mesoscale patches of enhanced or reduced soil moisture are performed. Boundary-layer clouds developed in all simulations. To assess the deviations of cloud cover on different scales within the model domain, we calculated the root-mean-square deviation (*RMSD*) between the sensitivity experiments and the reference simulation. The *RMSD* depends strongly on the spatial resolution at which cloud fields are compared. Different spatial resolutions of the cloud fields were generated by applying a low-pass filter. For all sensitivity experiments, large *RMSD* values occur for cut-off wavelengths $< 1 \text{ km}$, reflecting the stochastic nature of convection, but they decrease rapidly for wavelengths between 1 and 5 km. For cut-off wavelengths $> 5 \text{ km}$, the *RMSD* is still pronounced for the simulation with higher mean soil moisture. Additionally, for cut-off wavelengths between 5 and 30 km, considerable differences can be found for the experiment with mesoscale patches and for that with homogeneous land-surface parameters. Spatial averaging of land-surface parameters for areas of $2.5 \text{ km} \times 2.5 \text{ km}$ and $10 \text{ km} \times 10 \text{ km}$ results in larger patch sizes but simultaneously in reduced amplitudes of land-surface parameter anomalies and shows the lowest *RMSD* for all cut-off wavelengths.

✉ Leonhard Gantner
leonhard.gantner@kit.edu

¹ Institute of Meteorology and Climate Research, Karlsruhe Institute of Technology (KIT),
Postbox 3640, 76021 Karlsruhe, Germany

² Deutscher Wetterdienst, Offenbach, Germany

Keywords High-definition clouds and precipitation for advancing climate prediction (HD(CP)²) · High resolution modelling · Real-data large-eddy simulation · Soil moisture

1 Introduction

Soil properties such as soil moisture and soil type, as well as land-use properties such as plant cover and leaf area index (*LAI*), determine the partitioning of the available energy into the turbulent surface fluxes of sensible and latent heat. These turbulent fluxes represent the lower boundary conditions for the evolution of the convective boundary layer (CBL). Past results show that surface heterogeneities based on soil properties or vegetation affect both the cloud-free CBL (Wetzel and Chang 1988; Siebert et al. 1992; Sun and Bosilovich 1996; Raasch and Harbusch 2001; Pielke 2001; Maronga and Raasch 2013) and cloud-topped CBL (Rieck et al. 2014; Lohou and Patton 2014). For the cloud-topped CBL, surface-atmosphere feedbacks due to radiative effects of clouds on the surface energy balance and on the boundary layer have to be considered as well (Huang and Margulis 2013; Rieck et al. 2015). The spatial extent of land-surface anomalies is considered crucial for the development of secondary circulations. Spatial heterogeneities, e.g. of soil moisture from scales of the order of 2.5–10 km and above, often generate thermally-induced circulations similar to sea-breeze flows (e.g., Shuttleworth 1991; Courault et al. 2007). This is shown in observations (Taylor et al. 2007; Dixon et al. 2013) and in modelling studies (Ookouchi et al. 1984; Segal and Arritt 1992; Gantner and Kalthoff 2010; Garcia-Carreras et al. 2011; Adler et al. 2011). The circulation systems then introduce additional mesoscale differences to the CBL state. To resolve these processes in numerical simulations, the grid spacing of the applied model has to be appropriate. In recent years, the grid spacing of high-resolution and numerical weather prediction (NWP) models has decreased, implying that model resolution is of the same order of magnitude or even higher than the horizontal resolution of soil properties and land use. Thus both model grid spacing and land-surface parameter resolution may influence the simulated CBL.

Several authors investigated the impact of grid spacing on atmospheric processes and the cloud-topped CBL (e.g., Larson et al. 2012; Barthlott and Hoose 2015). Petch et al. (2002) found that a grid spacing of one quarter to one eighth of the sub-cloud-layer depth is necessary to simulate CBL clouds realistically. Honnert et al. (2011) showed that the resolved part of turbulent energy must be as large as the subgrid-scale (SGS) part if the grid-point distance is equal to a fifth of the depth of a dry CBL, and more if a cloud layer is present. Other studies investigated the impact of land-surface patterns of different length scales, e.g. artificial chess-board patterns or prescribed surface fluxes, on the CBL and on boundary-layer clouds (Shen and Leclerc 1995; Garcia-Carreras et al. 2011; Rieck et al. 2014; van Heerwaarden et al. 2014).

Recently, several studies (Catalano and Moeng 2010; Langhans et al. 2012; Hanley et al. 2015; Stein et al. 2015) made use of operational NWP models [e.g. the Weather Research and Forecast (WRF) model, the Consortium for Small Scale Modeling (COSMO) model, and the Met Office's Unified Model (UM)] in large-eddy simulation (LES) mode, i.e. operating with grid-point distances between 50 m and 500 m and using three-dimensional (3-D) turbulence parametrizations similar to those developed for large-eddy simulation (LES) models (e.g., the typical Smagorinsky schemes). Talbot et al. (2012) showed that simulations with the fine-resolution WRF model in LES mode are optimum for resolving small-scale surface features over heterogeneous surfaces.

In the past, less attention was paid to the influence of land-surface parameters, especially their spatial resolution, on the CBL in large-eddy simulations. In order to find out the relevant resolution, the following questions are addressed in this investigation: what is the impact of

soil- and vegetation-related parameter resolutions on the simulated cloud-topped CBL? How does this impact compare to that of areal-mean soil-moisture changes and enhanced soil-moisture anomalies? How does the comparison of cloud fields depend on their considered spatial resolution? To answer these questions, high-resolution (100-m grid spacing) real-data model simulations with realistic heterogeneous surface conditions, typical for a central European area, have been performed. In the experiments the resolution of soil- and vegetation-related parameters was modified. In addition, the mean soil moisture was varied and patches with enhanced/reduced soil moisture were implemented. The paper is structured as follows: Sect. 2 describes the model set-up and gives an overview of the simulations performed. Section 3 presents the sensitivity of the energy balance components, mean and turbulent CBL conditions and cloud-cover distribution to the land-surface parameter modifications. Finally, a summary and conclusions are given in Sect. 4.

2 Model Set-Up and Sensitivity Experiments

2.1 The COSMO Model in LES Mode

We use the COSMO model version 5.0 (Schättler et al. 2014), which is a fully compressible non-hydrostatic model used for NWP as well as for scientific applications down to high resolution. Here it is applied in a one-way nesting mode down to a resolution of 100-m horizontal grid spacing. A hybrid coordinate system with 80 layers is used in the vertical for all our experiments. The horizontal differencing is done on a rotated latitude/longitude grid using an Arakawa C-grid and a generalized terrain following height coordinate. The model is convection-resolving at this high horizontal resolution and therefore the convection parametrization is not used. A third-order Runge–Kutta scheme is used for time integration together with a fifth-order advection scheme; For scalar advection a second-order Bott scheme with Strang splitting is applied. The model is run with a complete physical parametrization package including the radiation scheme of Ritter and Geleyn (1992). This scheme is based on a delta two-stream version of the general equation for radiative transfer and considers three shortwave and five longwave spectral intervals. Clouds, aerosol and water vapour are treated as optically active constituents of the atmosphere and can therefore modify the radiative fluxes by absorption, emission and scattering. A new treatment of ice particles has been introduced as an extension of the original scheme. In order to allow for a rapid update of newly formed clouds the scheme is called every 3 min. For microphysics a bulk scheme considering rain, cloud water, cloud ice, graupel, and snow is applied. Initial and boundary data are typically taken from a driving host model and by using a Davies-type formulation for one-way nesting at the lateral boundaries, information from the driving model is fed to the model continuously. This is in contrast to the periodic lateral boundary conditions often used in a LES model. With these boundary conditions, we are able to simulate the CBL in a more realistic set-up; e.g., we may have an inhomogeneous horizontal CBL, implying that atmospheric variables at the inflow boundary can be quite different from those at the outflow boundary. The occurrence of clouds is determined by liquid water content. The lower boundary conditions for the atmospheric part of the model comprise the turbulent surface fluxes, whose calculation requires knowledge of soil moisture and soil temperature. These are determined with the Soil-Vegetation-Atmosphere Transfer multi-layer model, TERRA-ML (Heise 2002), which describes various thermal and hydrological processes within the soil. To link soil-texture with the corresponding hydraulic properties of the soil, we use regression relationships (pedotransfer functions) for the determination of van Genuchten parameters

(van Genuchten 1980) from fractions of silt, sand, clay, organic matter, and bulk density according to Wösten et al. (1999). This allows calculation of the soil moisture depending on nearly continuous soil properties (see, e.g., Smiatek et al. 2016) instead of using a few soil-texture based soil types, as valid for the standard version of the TERRA-ML model (e.g. Kohler et al. 2012). Thereby, the spatial averaging of the soil properties needed in our investigation becomes possible.

A 3-D turbulence parametrization scheme after Herzog et al. (2002b) is used as in Fiori et al. (2010). The parametrization of SGS turbulence is basically a prognostic turbulent kinetic energy (TKE) scheme, taking into account the three spatial directions (Herzog et al. 2002b). The turbulence diffusion coefficients of momentum and heat (K_m and K_h respectively) used in the 1.5-order closure to calculate the three-dimensional fluxes of momentum, heat, and moisture, are defined as

$$K_m = \Phi_m \Lambda \bar{e}^{1/2}, \quad (1)$$

$$K_h = \Phi_h \Lambda \bar{e}^{1/2}. \quad (2)$$

The functions Φ_m and Φ_h were derived using an extension of the Smagorinsky scheme as proposed by Mason (1994) and Mason and Brown (1999), and depend mainly on the local Richardson number. For more details, see Herzog et al. (2002a, b). The length scale Λ is a function of horizontal as well as vertical grid size, while the TKE per unit mass, \bar{e} , is retrieved from a prognostic equation.

2.2 Model Set-Up

Initial and lateral boundary conditions of the atmospheric part of the model are obtained from operational analyses of the COSMO-DE model. This is the operational convection-permitting NWP model of the German Weather Service (DWD) with 0.025° (about 2.8 km) grid-point distance (e.g. Baldauf et al. 2011). A first COSMO model simulation with 500-m grid spacing is initiated at 0000 UTC on 5 May 2013 and the boundary conditions are updated every hour. This day was selected from the High Definition Clouds and Precipitation for Climate Prediction (HD(CP)²) observational prototype experiment (HOPE, e.g. Macke et al. 2017; Maurer et al. 2016) because CBL clouds developed and the wind speed in the CBL was small (about 3 m s⁻¹). Thus large-scale advection should not dominate the impact of surface fluxes on the CBL evolution. The model domain for the 500-m simulation contains 401 × 461 grid points and extends from 4.5°E to 7.6°E and from 49.6°N to 51.9°N. The high-resolution simulation is nested into the domain with 500-m grid spacing with an update frequency of 15 min for the boundaries and has a horizontal grid spacing of 0.001° (about 100 m). The same settings for physical processes and turbulent diffusion are used in the 500- and 100-m simulations. Both simulations use a rotated coordinate system with the North Pole at 40°N and 170°W. The inner domain has 701 × 661 grid points horizontally and encompasses a region (including the HOPE area) in north-western Germany from about 5.6°E to 6.7°E and from 50.4°N to 51.05°N, i.e. 70 × 70 km² (Fig. 1). The evaluation area is somewhat smaller and stretches from 5.7°E to 6.6°E and from 50.45°N to 51.0°N. Of the 80 layers in the vertical, used in both the 100- and 500-m simulations, 40 (30) layers are in the first 3000 (1500) m above ground with the lowest at 10 m. The separation of layers increases with height.

For orography, we use the high resolution Advanced Spaceborne Thermal Emission and Reflection Radiometer (ASTER) dataset, which is available at a resolution of 30 m. Soil parameter data with a resolution of about 1 km are taken from the Harmonized World Soil Database (HWSD, Nachtergaele et al. 2012). Information about land use is taken from the

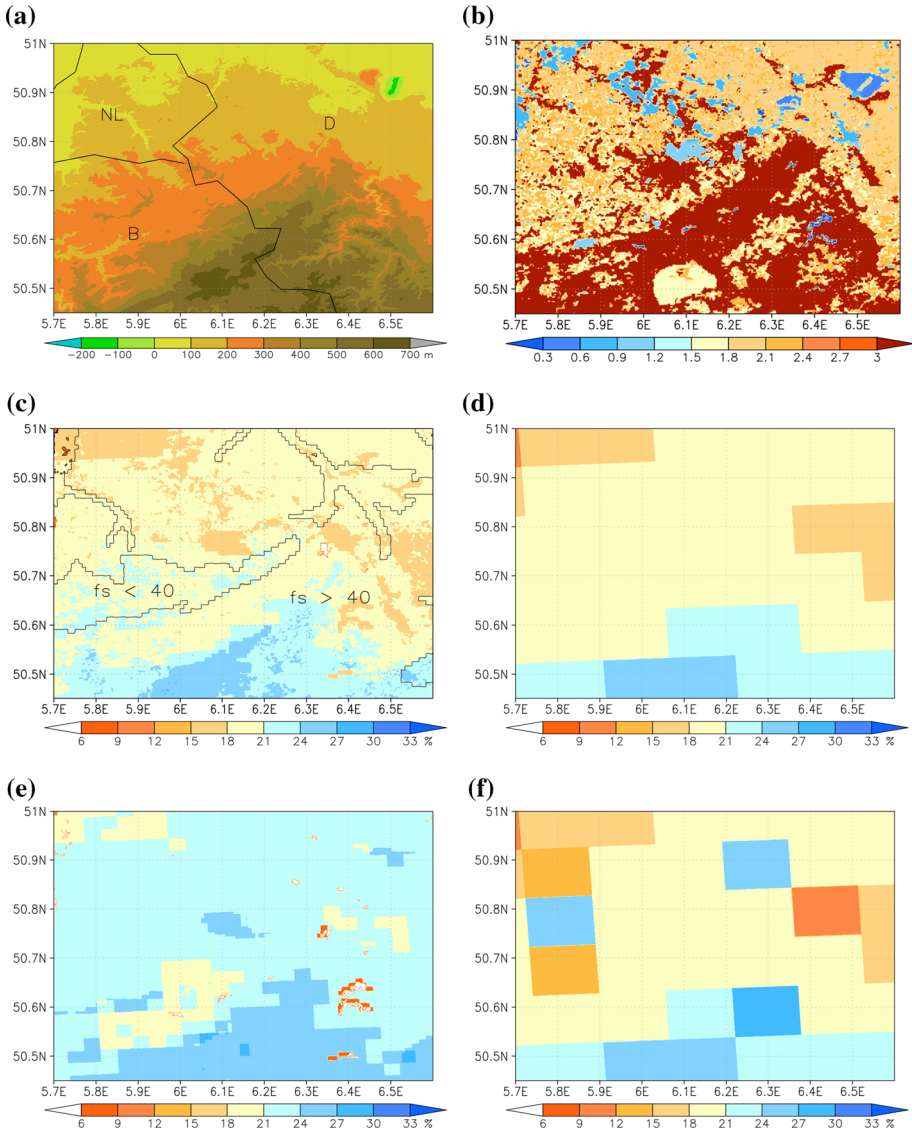


Fig. 1 Orography in m (colour coded), with black lines marking borders between Germany (D), Belgium (B) and the Netherlands (NL) (a), LAI (b), initial soil moisture in the uppermost 10-mm layer (colour coded) and overlaid fraction of sand (f_s) for the *ref* simulation (c) and initial soil moisture for the *s100/sv100* (d), for the *desoi* (e), and for the *svmod* (f) experiments with 100-m grid spacing

European Space Agency GLOBCOVER dataset with 300-m resolution. These data are prepared with a preprocessor for use in the COSMO model, and is done separately for both domains. For the initialization of soil moisture and soil temperature, the TERRA-ML model was run in stand-alone mode starting at the beginning of March for the 100-m simulation model domain, using the corresponding soil and vegetation parameters and orography dataset. The TERRA-ML model run was forced by the COSMO-DE model analyses and precipita-

Table 1 List of sensitivity experiments

Abbreviation	Description
<i>ref</i>	Vegetation and soil data with highest available resolution
<i>v25</i>	Vegetation averaged over 25×25 grid points
<i>s25</i>	Soil data averaged over 25×25 grid points
<i>v100</i>	Vegetation averaged over 100×100 grid points
<i>s100</i>	Soil data averaged over 100×100 grid points
<i>sv100</i>	Vegetation and soil data averaged over 100×100 grid points
<i>vcon</i>	Vegetation averaged over the whole modelling domain
<i>scon</i>	Soil data averaged over the whole modelling domain
<i>svcon</i>	Soil and vegetation averaged over the whole modelling domain
<i>svmod</i>	Six patches with increased and decreased soil moisture
<i>desoi</i>	Soil moisture interpolated from COSMO-DE analysis data

tion observed by the DWD radar network. This allows more highly resolved soil-moisture information than provided by the COSMO-DE model forecast; additionally, the soil moisture is better adapted to the HWSD-derived soil parameters. For another simulation, we interpolated the soil moisture of the COSMO-DE model forecast to the 100-m grid. These data are used to investigate the effect of a different soil moisture content on CBL cloud evolution.

2.3 Overview of Simulations

For the reference simulation (henceforth denoted as *ref*), we used the highest available resolutions for land use, vegetation and soil properties (see previous Section). The fraction of sand, *LAI*, and the initial fields of volumetric soil moisture content in the uppermost layer of 10 mm are shown in Fig. 1. The fraction of sand exceeds 40% in a substantial part of the modelling domain (Fig. 1c). In the northern part of the domain, the orography is fairly flat (about 100 to 200 m above mean sea level, m.s.l.) while it is hillier in the southern part (about 400 to 600 m above m.s.l.; Fig. 1a). The hilly area is covered mainly with forests, reflected by higher *LAI* values (Fig. 1b). The soil moisture in the uppermost 10-mm layer ranges from around 12% in the northern part to around 26% in some southern parts, and the soil moisture increases with depth. The root-zone soil moisture has a similar but smoother distribution than that in the uppermost layer (not shown). No mesoscale patches with pronounced higher or lower soil moisture were present, because there was almost no precipitation during the previous weeks (e.g. Maurer et al. 2016).

For the various sensitivity experiments performed for the 100-m simulation, we averaged some or all of the soil and vegetation data over 25×25 and 100×100 grid point boxes and over the whole modelling domain. Averages over the whole domain are henceforth denoted as areal means. Table 1 summarises the various sensitivity experiments, noting that the initial areal mean of individual land-surface parameters is the same in all experiments. For example the areal mean of the initial soil moisture of the *ref*, *s25*, and *s100* experiments is equal to the initial soil moisture of the *scon* experiment. Overall, we performed the reference simulation and 10 sensitivity experiments, with the land-surface properties divided into two groups. The first is vegetation, which is represented in the TERRA-ML model as plant cover, *LAI*, root

depth and albedo. In the second we cover all soil-related properties: the percentage of sand, silt, clay and organic matter as well as soil moisture and soil temperature. The experiments are denoted as follows: the 25×25 grid point ($\approx 6.25 \text{ km}^2$) soil/vegetation averages as $s25/v25$, the 100×100 grid point averages ($\approx 100 \text{ km}^2$) as $s100/v100$ and the experiments with uniform values as $scon/vcon$, respectively. For example, the resulting soil moisture distribution for the $s100$ experiment is shown in Fig. 1d. When both quantities, i.e. soil and vegetation, are averaged over 100×100 grid points we call the experiment $sv100$. In the $svcon$ experiment the land-surface parameters are constant for the whole domain. In an additional experiment, the soil moisture in three 100×100 grid point boxes (arbitrarily distributed in the model domain) is enhanced and reduced by 30%, respectively, in order to have pronounced horizontal soil moisture gradients. By this, the soil moisture in the uppermost layer of 10-mm ranges from 9 to 29%, i.e. the span is less than the one of the high-resolution soil moisture field (*ref*) but greater than the one with equal resolution ($s100$). These conditions should represent soil-moisture anomalies as typically generated by convective precipitating systems (e.g. Schwendike et al. 2010; Kohler et al. 2010; Khodayar et al. 2013). This experiment is denoted as $svmod$ and its soil moisture distribution is shown in Fig. 1f. Finally, we interpolated the soil moisture directly from the COSMO-DE model for one experiment and named it *desoi* (Fig. 1e). As mentioned above, the initial areal-mean soil moisture is the same for all experiments (18.5%) except for the *desoi* experiment, for which the areal mean value is 20.8%.

The impact of averaging the soil and vegetation properties on the spectrum of the soil and vegetation fields is analyzed applying fast Fourier transform (Fig. 2). Averaging soil and vegetation properties results not only in the cut off of small-scale structures but also in a reduction of the spatial amplitudes (Fig. 2c,d). For example, the soil-moisture amplitude is about 23% (max = 27.5%, min = 4.9%) in the *ref* simulation, 19% (max = 26%, min = 7.3%) in the $s25$ experiment, and 16% (max = 25%, min = 9%) in the $s100$ experiment. This also becomes visible in the meridional cross-sections of the LAI distribution in the *ref*, $v25$, and $v100$ simulations and of the soil-moisture distribution in the *ref*, $s25$, and $s100$ simulations (Fig. 2a, b). Reducing the land-surface parameter differences between mesoscale structures also reduces their ability to generate secondary circulations. The heterogeneity length scale and span of land-surface parameter values are also identified by Huang and Margulis (2013) as relevant factors for cloud-cover evolution. Figure 2d also includes the soil-moisture spectrum for the $svmod$ experiment. The implementation of areas with pronounced soil-moisture anomalies (amplitude of 20%) with side lengths of 10 km produces an increase of the spectral energy at the corresponding wavelengths compared to the ones of the *ref*, $s25$, and $s100$ simulations (Fig. 2d).

3 Results

A surface anticyclone with one centre over northern France and the other one over the Baltic States (not shown) dominated the conditions in the investigation area on 5 May 2013, so that a moderate south-westerly flow with wind speeds $\approx 3 \text{ m s}^{-1}$ is present in the CBL. The centre of the accompanying upper level ridge is positioned over western Scandinavia so that south-south-westerly flow prevailed above the CBL. With this, a horizontal potential temperature gradient of about $4 \text{ K} (100 \text{ km})^{-1}$ and a specific humidity gradient of $1 \text{ g kg}^{-1} (100 \text{ km})^{-1}$ from north-north-west to south-south-east was present in the boundary layer of the model domain. Cumulus clouds formed in the course of the day.

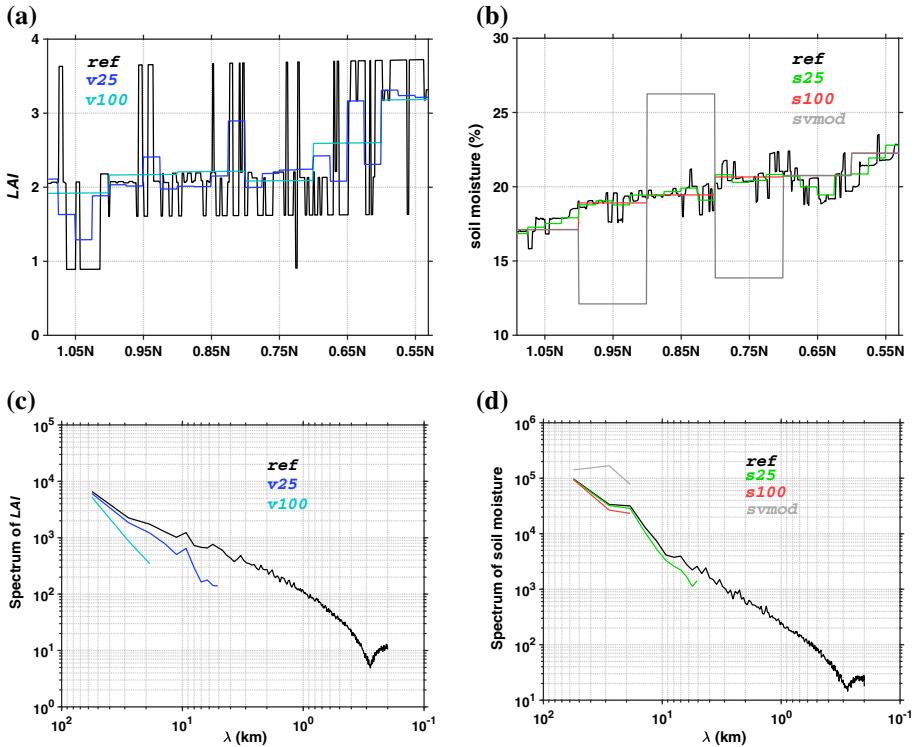


Fig. 2 Values of LAI (a) and soil moisture (b) for the *ref*, *v25*, *v100* and *ref*, *s25*, *s100*, and *svmod* simulations, respectively along a south-north cross-section at 5.82°E (see Fig. 1). Spectra of LAI for the *ref*, *v25*, and *v100* simulations (c) and of soil moisture for the *ref*, *s25*, *s100*, and *svmod* simulations (d)

3.1 The Surface Energy Balance Components

The areal-mean energy balance components of the *ref* simulation are shown in Fig. 3a. At 1200 UTC, the net radiation, Q_0 , attains a value of 589 W m^{-2} , and a large proportion of the available energy is manifest as the sensible heat flux, H_0 , which is about 270 W m^{-2} , so that the Bowen ratio $\beta = 1.43$. The sensitivity experiments, where the land-surface parameters are averaged (i.e. the *s25*, *s100*, *scon*, *v25*, *v100*, *vcon*, *sv100*, and *svcon* experiments) or modified (*svmod* experiment), exhibit very similar time series (not shown). For example, at 1200 UTC in the *svcon* experiment, $Q_0 = 591 \text{ W m}^{-2}$, $H_0 = 279 \text{ W m}^{-2}$ and $\beta = 1.45$ and in the *svmod* experiment, $Q_0 = 592 \text{ W m}^{-2}$, $H_0 = 280 \text{ W m}^{-2}$ and $\beta = 1.5$ (Fig. 3c). As a result the mean heat supply into the atmosphere in these sensitivity experiments is only slightly higher than in the *ref* simulation. Only in the *desoi* experiment is a considerably lower amount of available energy transferred into sensible heat (at 1200 UTC, $H_0 = 226 \text{ W m}^{-2}$) so that $\beta = 0.95$ (Fig. 3c).

Although considerable differences for the areal-mean surface fluxes only occur for the *desoi* experiment, spatial differences can be found for all sensitivity experiments. The histogram in Fig. 3b illustrates the frequency distributions of H_0 in the model domain at 1200 UTC exemplarily for the *ref*, *svcon*, *svmod* and *desoi* simulations. In the *ref* simulation, the values of H_0 vary between about 175 and 350 W m^{-2} , with $H_0 \approx 270 \text{ W m}^{-2}$ at the

majority of the model grid points. The experiment with completely uniform land-surface conditions (*svcon* experiment) exhibits a reduction in spatial variability; grid points with lower flux values (H_0 between 200 and 250 W m^{-2}) are reduced while more grid points with $H_0 = 250$ to 300 W m^{-2} appear (Fig. 3d) so that more grid points have values close to the areal mean (Fig. 3b). The impact of orography and clouds mainly prevents a uniform distribution of H_0 in the *svcon* experiment at noontime, as seen from inspection of the spatial sensible-heat-flux pattern (Fig. 3f). In the *svmod* experiment, the implemented soil-moisture anomalies produce several additional small peaks in the H_0 distribution, e.g. at its lower (around 130 W m^{-2}) and higher (about 400 W m^{-2} and 470 W m^{-2}) range (Fig. 3b, d). In total, the areal-mean sensible heat flux is 10 W m^{-2} higher than in the *ref* simulation. In the *desoi* experiment, the histogram shows a shift of the H_0 maximum by about -50 W m^{-2} compared to the *ref* simulation (Fig. 3b, d), due to the higher soil moisture. The width of the distribution is slightly narrower than for the *ref* simulation. The same characteristics hold for E_0 distributions (not shown). These inner-domain flux characteristics affect the mean and turbulent CBL conditions as well as the cloud distributions, as can be seen below.

3.2 The Mean CBL Conditions

The vertical profiles of areal-mean specific humidity, q , and potential temperature, Θ at 1000, 1200 and 1400 UTC show that the mixed-layer top rises from about 900 m up to about 1500 m between 1000 UTC and 1400 UTC (Fig. 4a, c). The CBL-capping inversion covers a layer of several hundreds of metres. In the mixed layer, the specific humidity does not increase significantly with time but is mixed over higher layers during the course of the day. Cumulus clouds form in this growing part of the CBL where q increases; the liquid water content, lwc , reaches its maximum at 1200 UTC (Fig. 4a, c).

The areal-mean differences of specific humidity, Δq , between the various sensitivity experiments and the *ref* simulation in the mixed layer at 1200 UTC range from about $\Delta q = -0.03 \text{ g kg}^{-1}$ for the *svcon* experiment to $\Delta q = +0.17 \text{ g kg}^{-1}$ for the *desoi* experiment (Fig. 4b). The areal-mean potential temperature differences, $\Delta\Theta$, span from about $\Delta\Theta = +0.1 \text{ K}$ for the *svcon* experiment to about $\Delta\Theta = -0.3 \text{ K}$ for the *desoi* experiment (Fig. 4d). In the surface layer, the deviations of q and Θ are often somewhat greater. Large Θ and q differences are seen also between heights of 1500 to 1800 m, i.e. in the capping-inversion layer; e.g. areal-mean Δq is up to $+0.11 \text{ g kg}^{-1}$ for the *svcon* experiment and up to $\pm 0.13 \text{ g kg}^{-1}$ for the *desoi* experiment (Fig. 4b). The potential temperature differences, $\Delta\Theta$, range from about $\Delta\Theta = -0.17 \text{ K}$ for the *svcon* experiment to about $\Delta\Theta = +0.38 \text{ K}$ for the *desoi* experiment (Fig. 4d), due to the different CBL depths. Negative/positive peaks of $\Delta\Theta$ correspond to a higher/lower CBL depth compared to the *ref* simulation. Thus, in the *svcon* experiment the mixed layer is warmer and dryer and the CBL is deeper than in the *ref* simulation, while in the *desoi* experiment the mixed layer is colder and moister and the CBL is about 200 m shallower than in the *ref* simulation. These different mean CBL conditions are ascribed to the corresponding surface conditions. For example, the deeper and warmer CBL in the *svcon* experiment is assigned to the higher sensible heat fluxes (see Sect. 3.1) while the lower and colder CBL in the *desoi* experiment is due to the lower sensible heat flux (Fig. 3b).

3.3 The Turbulent CBL Characteristics

Turbulent characteristics in the CBL are investigated based on the spatial standard deviations of potential temperature, σ_Θ , specific humidity, σ_q , and vertical velocity, σ_w (Fig. 5).

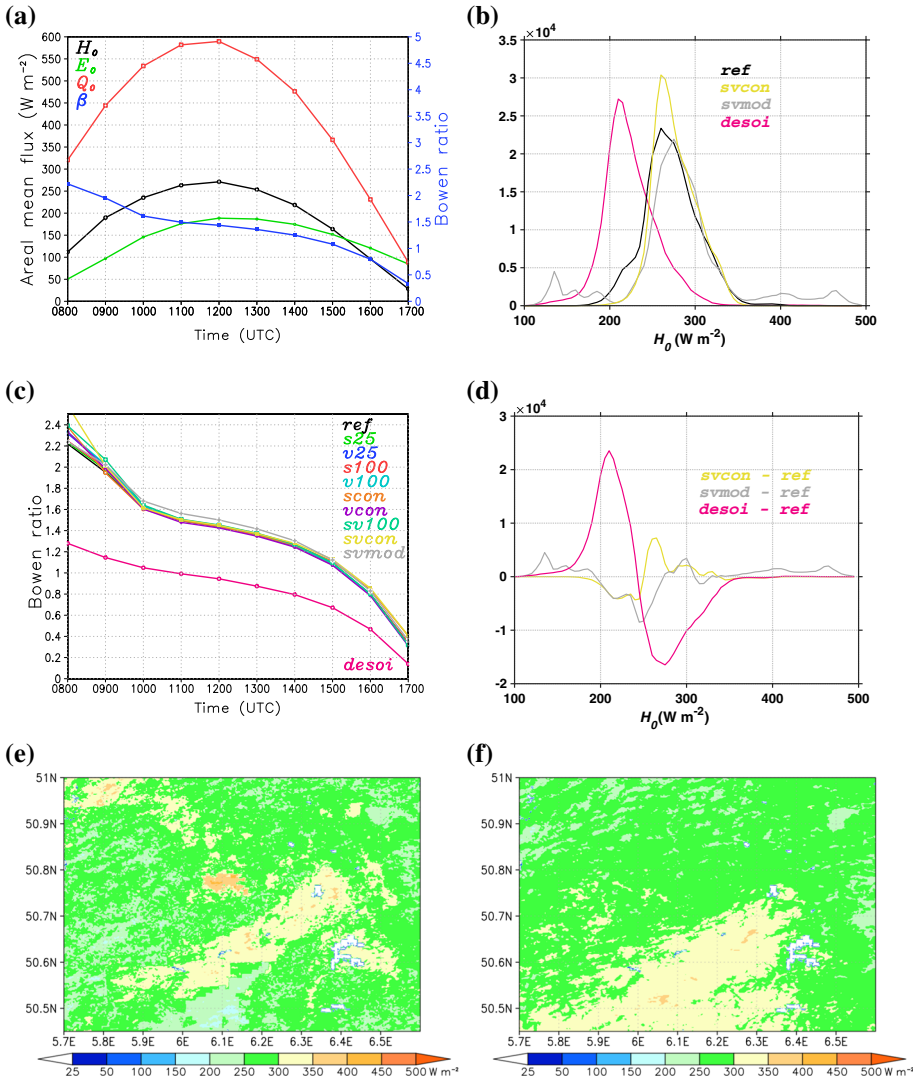


Fig. 3 Time series of the areal-mean net radiation, Q_0 , sensible, H_0 , and latent heat flux, E_0 , and Bowen ratio, β , for the *ref* simulation (a). Histogram showing the distribution of H_0 in the *ref*, *svcon*, *svmod*, and *desoi* simulations in the model domain at 1200 UTC (b). Time series of the areal-mean Bowen ratio, β , for the *ref*, *s25*, *v25*, *s100*, *v100*, *scon*, *vcon*, *sv100*, *svcon*, *svmod*, and *desoi* simulations (c). Histogram showing the distribution of H_0 differences between the *svcon*-*ref*, *svmod*-*ref* and *desoi*-*ref* simulations in the model domain at 1200 UTC (d). Spatial distribution of the sensible heat flux for the *ref* simulation (e) and for the *svcon* experiment (f) at 1200 UTC

As is clear from Fig. 4, the profiles of σ_θ and σ_q exhibit maxima at the top of the CBL and within the cloud layer, respectively, while in the sub-cloud layer the values are considerably smaller (Fig. 5a, b). These results are consistent with previous studies (e.g. Caughey 1982; Garratt 1994), turbulence measurements (Maurer et al. 2016) and large-eddy simulations (Heinze et al. 2017) for the HOPE campaign. In the mixed layer, the sensitivity experiments

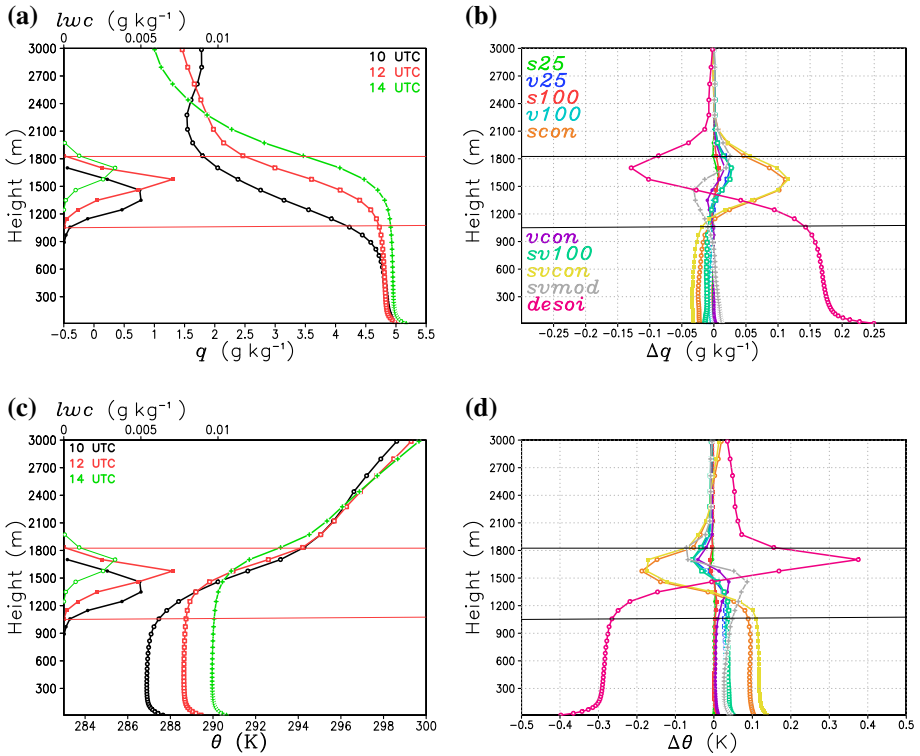


Fig. 4 Profiles of specific humidity, q , potential temperature, θ , and liquid water content, lwc , at 1000, 1200, and 1400 UTC (a, c) in the *ref* simulation as well as the humidity Δq and temperature $\Delta\theta$ differences between the various sensitivity experiments and the *ref* simulation at 1200 UTC (b, d)

with uniform land-surface conditions (*scon*, *svcon*) produce somewhat higher σ_θ values ($\Delta\sigma_\theta = +0.12\ K$, Fig. 5c, d). Compared to the *ref* simulation, *LAI* and soil moisture values in the *scon* and *svcon* experiment are lower in the southern and higher in the northern part of the model domain (Fig. 2). This larger-scale feature determines the spatial distribution of the sensible heat flux (Fig. 3f) and produces a corresponding larger-scale temperature gradient in the mixed layer (warmer in the south and colder in the north), which results in higher $\Delta\sigma_\theta$ values compared to the *ref* simulation. Large differences between the various sensitivity experiments exist at the CBL top and in the inversion layer (Fig. 5b, d). These are due to the different CBL depths and stronger convection in the CBL.

The σ_w profiles for the various sensitivity experiments (Fig. 5e) all show the typical vertical structure with maxima in the lower part of the CBL (Lenschow et al. 1980) and then σ_w values decreasing until about 1500 m; σ_w remains nearly constant up to about 1800 m and then decreases at higher levels. The occurrence of higher σ_w values within the cloud layer is in agreement with observations (e.g. Lenschow et al. 2012). The simulated maximum values of about $\sigma_w = 1.5\ m\ s^{-1}$ also agree with observations performed on that particular day in the model domain (not shown). The enhanced turbulence is assigned to latent heat release in conjunction with cloud formation. The greatest difference between the various σ_w profiles exists for the *desoi* experiment (Fig. 5f). The σ_w values are lower than for the other sensitivity

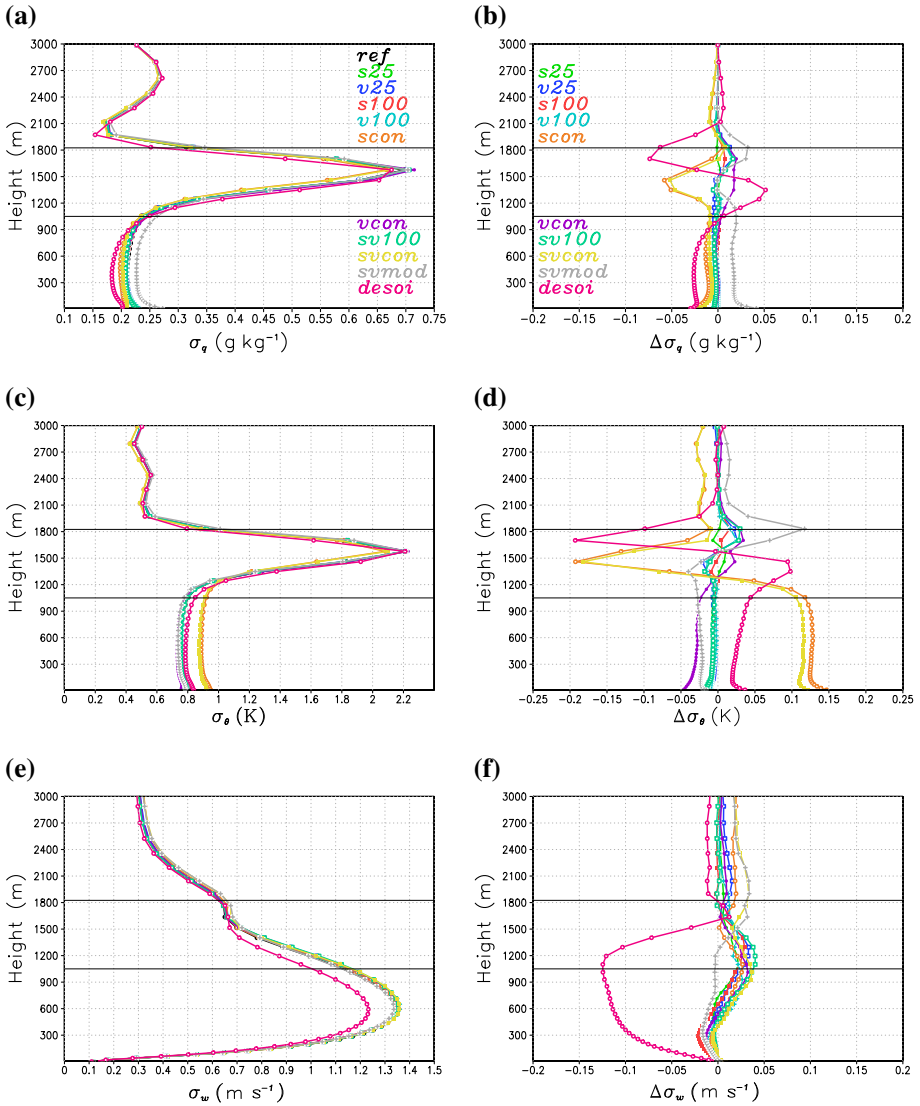


Fig. 5 Profiles of the spatial standard deviation of the specific humidity, σ_q (a), potential temperature, σ_θ (c), and the vertical velocity, σ_w (e), and the corresponding differences between the various sensitivity experiments and the *ref* simulation (b, d, f). All profiles are for 1200 UTC. The two horizontal black lines mark the top and bottom of the cumulus-cloud layer

experiments because of the reduced sensible heat flux (Fig. 3b), i.e. there is less surface-based buoyancy-driven turbulence.

Additional insight into the σ_w differences generated in the various simulations is provided by the vertical velocity spectra (Fig. 6a), determined from north-south and east-west oriented sequences of w at 1200 UTC at about a height of 600 m, i.e. approximately in the middle of the sub-cloud layer (Fig. 5e). The spectra of the *ref*, *svmod* and *desoi* simulations are representative of different sensitivity experiments. The spectra show that the wavelength, λ ,

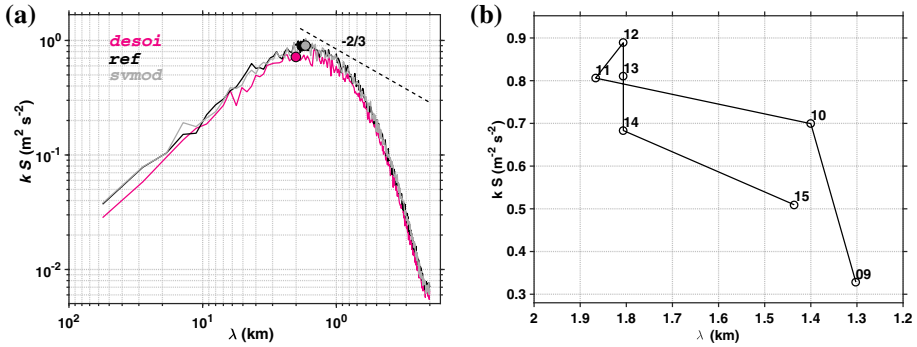


Fig. 6 Spectral density, $k S$, of the vertical velocity component derived from north-south and west-east oriented sequences at about 600 m for the *ref*, *svmod* and *desoi* simulations at 1200 UTC (a). The $-2/3$ slope in the inertial subrange is additionally indicated in the diagrams of the spectra. Dots mark the maxima of $k S$. Maximum spectral densities and corresponding wavelength of the *ref* simulation at a height of about 600 m for various times (b)

at which the maximum energy occurs ranges from about $\lambda = 2$ km in the *desoi* experiment to about $\lambda = 1.7$ km in the *ref* simulation (Fig. 6a). At this time, the spectral density, $k S$, reaches its maximum, e.g. $k S \approx 0.9 \text{ m}^2 \text{ s}^{-2}$ in the *ref* simulation (Fig. 6b). The spectral density of the *desoi* experiment, especially at greater wavelengths ($\lambda > 20$ km), is somewhat lower than for the other two experiments (Fig. 6a). This indicates that the lower σ_w values in the *desoi* profile (Fig. 5e) are mainly due to a smaller contribution of spectral density at greater wavelengths. Turbulence spectra also show that a large part of the turbulent energy is resolved at the energy-containing scales. For wavelengths corresponding to about $10\Delta x$, i.e. 1 km and lower, the decrease of energy is much too large compared to the theoretical $-2/3$ slope in the inertial sub-range. This is related to the 5th-order advection scheme, see [Shin and Hong \(2013\)](#) and [Ricard et al. \(2013\)](#).

3.4 Cloud Cover

3.4.1 Mean Differences

In order to assess the impact of land-surface parameter resolution on clouds, the areal-mean cloud cover is compared between simulations. Figure 7a shows the areal-mean cloud cover of the *ref* simulation and the areal-mean differences between the various sensitivity experiments and the *ref* simulation. In the *ref* simulation the cumulus clouds develop in the morning (at about 0900 UTC) and a maximum cloud cover of about 11% is reached between 1200 and 1300 UTC. In the afternoon, the cloud cover decreases continuously and clouds nearly vanish at about 1600 UTC. A representative example of the cloud field and the cloud-size distribution is given for 1200 UTC for the *ref* simulation (Fig. 8). About 400 cloud objects with a length dimension (the square root of the cloud area) of ≈ 0.1 km are simulated in the modelling domain (Fig. 8b). The largest clouds are 2.5 km wide. This decrease in cloud amount with increasing cloud length is typical of observed cumulus cloud fields ([Plank 1969](#); [Hozumi et al. 1982](#)). The comparison of the sensitivity experiments with the *ref* simulation reveals that most (*s25*, *v25*, *s100*, *v100*, *sv100*, *vcon*, and *svmod* experiments) show nearly no difference in areal-mean cloud cover ($\leq 1\%$, Fig. 7a). Slightly less clouds develop in the *scon*, *svcon* and *svmod* experiments than in the *ref* simulation for most of the time. Only the *desoi*

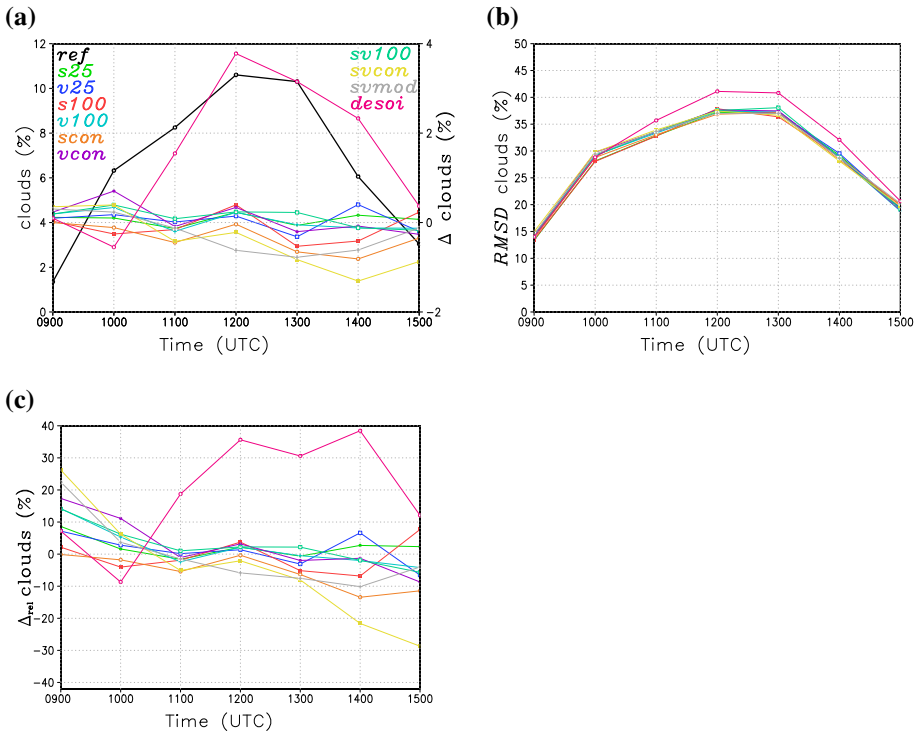


Fig. 7 Areal-mean cloud cover of the *ref* simulation (*bold black line*) for the whole domain and the differences (Δ clouds) of the various sensitivity experiments to the *ref* simulation (a). *RMSD* calculated from the various sensitivity experiments and the *ref* simulation (b). Relative differences of clouds of the various sensitivity experiments to the *ref* simulation (c)

experiment with the colder and more humid CBL produces a considerably higher amount of clouds (about +4% at 1200 UTC). The *desoi* experiment produces about 30–40% more clouds than the *ref* simulation in the early afternoon (Fig. 8c) relative differences, i.e. after normalization with the cloud cover of the *ref* simulation. In all other sensitivity experiments, the relative differences are considerably smaller.

This implies that the land-surface parameter resolution has a small impact on the evolution of the areal-mean cloud cover for those experiments for which the values of the areal-mean land-surface parameters at initiation time are equal. In these experiments, only small differences in the areal-mean net radiation and turbulent fluxes develop in the course of the day. However experiments with less clouds, e.g. *svcon*, have a (slightly) higher net radiation, a higher sensible heat flux, and a warmer CBL, which is unfavourable for cloud development. On the other hand, the increase of the areal-mean soil moisture from 19% in the *ref* simulation to 21% in the *desoi* experiment, produced a considerably higher areal-mean cloud cover.

3.4.2 Spatial Differences

For the assessment of the spatial differences of cloud cover between the various simulations, the root-mean-square deviation (*RMSD*) is calculated based on the differences between the cloud cover of the various sensitivity experiments and the *ref* simulation (Fig. 7b). The time

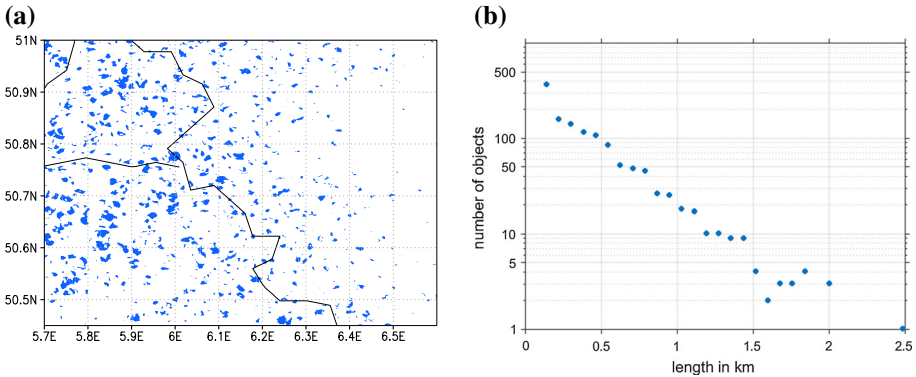


Fig. 8 Cloud distribution for the *ref* simulation at 1200 UTC (a). Cloud-size distribution (b) derived from the cloud field shown in (a)

series of the *RMSD* values for most of the cases are very similar, and the maximum *RMSD* $\approx 38\%$ appears at noon. The *RMSD* value of the *desoi-ref* experiment is somewhat higher than for the other ones (about 41%). To understand these spatial differences of the cloud-field distributions, the difference fields of cloud cover for three sensitivity experiments with pronounced deviations (*svcon*, *desoi*, and *svmod* experiments) are shown in Fig. 9a, c, e. These difference fields suggest that small displacements of the clouds between the different experiments contribute considerably to the large *RMSD* values, a contribution known as the “double penalty” effect. Spectral analyses of the cloud-difference fields using fast Fourier transform reveal a characteristic or dominant wavelength of about 3 km in this displacement (not shown). The difference fields also indicate that mostly positive values prevail in the *desoi-ref* experiment (Fig. 9c) while in the *svmod-ref* experiment, patterns exist where negative or positive values dominate (Fig. 9e).

Small displacements of clouds between the different experiments of the order of $\mathcal{O}(1\text{ km})$ are related to the stochastic nature of convection. Cloud-cover differences on the order of $\mathcal{O}(10\text{ km})$, however, are more relevant for most applications. To make those mesoscale patterns visible between the different cloud fields, the original cloud-cover fields are low-pass filtered by applying a filter wavelength of 10 km. The resulting difference fields for the *svcon-ref*, *desoi-ref*, and *svmod-ref* experiments are shown in Fig. 9b, d, f and reveal the following: (i) In the *svcon-ref* difference field, higher cloud cover occurs mainly in the north-north-western part while lower cloud cover can be found in the south-south-eastern part. The values are less than $\pm 15\%$. This pattern coincides roughly with the different H_0 pattern of the *ref* simulation and *svcon* experiment (Fig. 3e, f): in the *svcon* experiment, lower/higher H_0 values in the north-north-western/south-south-eastern part of the model domain produce lower/higher CBL temperatures and more/less clouds compared to the *ref* simulation. (ii) The *desoi-ref* difference field shows that more clouds occurred almost throughout the model domain (up to about 20% in some regions). This is consistent with the soil moisture being mostly larger in the whole model domain in the *desoi* experiment (Fig. 1c, e). (iii) The *svmod-ref* difference field indicates distinct spatial patterns, especially in the northern part where the orography is nearly flat (Fig. 1a). The length of the generated stripes of cloud-cover differences is several tenths of kilometres and they are oriented along the mean west-south-westerly wind direction. The width of the stripes is of the order of 10 km. Obviously, they are initiated over the downwind sides of implemented soil-moisture anomalies with higher/lower cloud cover downstream of patches with reduced/enhanced soil moisture. Inspection of the

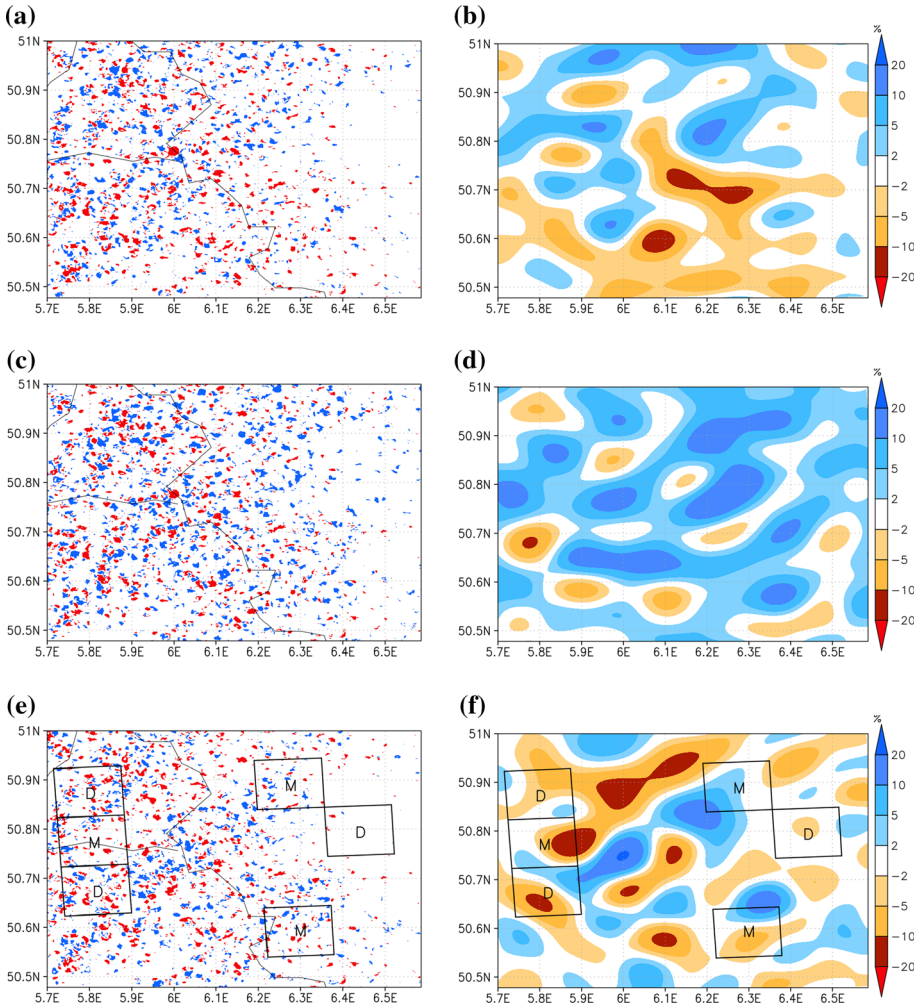


Fig. 9 Differences of cloud distribution for the *svcon-ref* (a), *desoi-ref* (c), and *svmod-ref* (e) simulations (positive/negative values shown in blue/red), and corresponding low-pass filtered (cut-off wavelength = 10 km) difference fields, respectively (b, d, f). All fields are for 1200 UTC

different parameters shows that patches with a lower soil moisture are accompanied by a higher surface sensible heat flux and vice versa (Fig. 10a). As a result, thermally-induced circulations are generated, causing strong divergence/convergence over and downstream of patches with a reduced/enhanced surface sensible heat flux (Fig. 10b). The highest convergence/divergence occurs preferentially over the transition zones from lower to higher and higher to lower soil moisture, respectively.

The areal-mean differences of cloud cover (Fig. 7) as well as the difference fields (Fig. 9a, c, e) indicate that the cloud-cover differences are influenced by land-surface parameters, but that the cloud-cover difference depends on the spatial resolution considered. We use the *RMSD* to quantify the amount of cloud-cover difference at different resolutions. To realise different spatial resolutions, we applied a low-pass filter with various cut-off wavelengths to the original cloud fields. The dependencies on the spatial resolution were calculated for the sensitivity

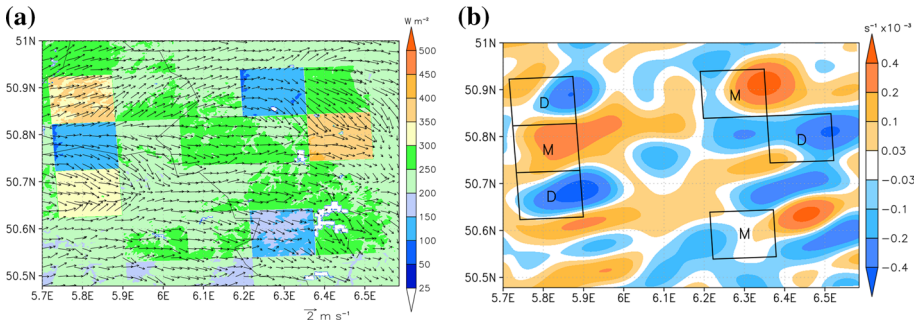


Fig. 10 Surface sensible heat flux and near-surface horizontal wind vector (a) and near-surface divergence for the *svmod* experiment (b). Data are averaged from 0900 UTC to 1500 UTC. The divergence field is low pass filtered with a cut-off wavelength of 10 km

experiments at 1200 UTC, i.e. when the *RMSD* reaches maximum values (Fig. 7b). In order to provide the results in a more general form, we additionally normalized the *RMSD* with the corresponding areal-mean cloud cover of the reference simulation (Fig. 7a). The normalized *RMSD* is denoted $RMSD_n$. The $RMSD_n$ for all cloud-cover differences, i.e. independent of the land-surface parameter resolution, decreases continuously with the increase of cut-off wavelength (Fig. 11). Applying cut-off wavelengths of $\lambda < 1$ km does not result in a considerable decrease in $RMSD_n$; the strongest decrease can be found between $\lambda \approx 1$ km and 5 km. For $\lambda < 1$ km, the $RMSD_n > 3$, i.e. it is still greater than the areal-mean cloud cover itself. This is because the displacements of individual clouds between the different sensitivity experiments, related to the stochastic nature of convection, dominate the $RMSD_n$ at this high spatial resolution. Recall that the dominant wavelength for the displacement of individual clouds is found to be $\lambda \approx 3$ km. Thus, at scales ≤ 3 km, the predictability for the location of clouds is low in a deterministic sense. For $\lambda > 5$ km, i.e. after crossing this critical wavelength, $RMSD_n < 1$ and considerable deviations between the various curves can be found. With respect to the various sensitivity experiments, the *desoi* experiment shows the largest $RMSD_n$ values at all wavelengths and remains > 0.4 . This is associated with the generally higher cloud cover in the whole model domain (Fig. 9d). Cloud patterns generated by secondary circulations, as valid for the *svmod* experiment (Fig. 9f), still result in higher $RMSD_n$ values at larger wavelengths (e.g. $5 \text{ km} < \lambda < 30 \text{ km}$) but nearly diminish for cut-off wavelengths of $\lambda > 30$ km. Sensitivity experiments with uniform land-surface parameter distributions (e.g. the *scon* and *svcon* experiments), which also resulted in mesoscale cloud-cover differences (Fig. 9b), show slightly higher $RMSD_n$ values for about $5 \text{ km} < \lambda < 30 \text{ km}$. The lowest $RMSD_n$ values can be found when the land-surface parameter resolution is only slightly lower than for the *ref* simulation (e.g. for the *s25* and *v25* experiments). No cloud-cover difference is generated on a scale of several kilometres so that the $RMSD_n$ value for $\lambda = 10$ km is already about 0.25. An increase of the heterogeneity-length scale and a reduction of the span of land-surface parameter values caused by averaging mainly compensate each other concerning the effects on cloud cover.

4 Summary and Conclusions

Sensitivity tests with the COSMO model in LES mode ($\Delta x = 100$ m) are performed to investigate the impact of changes in the resolution and absolute values of soil- and vegetation-related parameters on a cloud-topped boundary layer. The model is run in a real-data environment

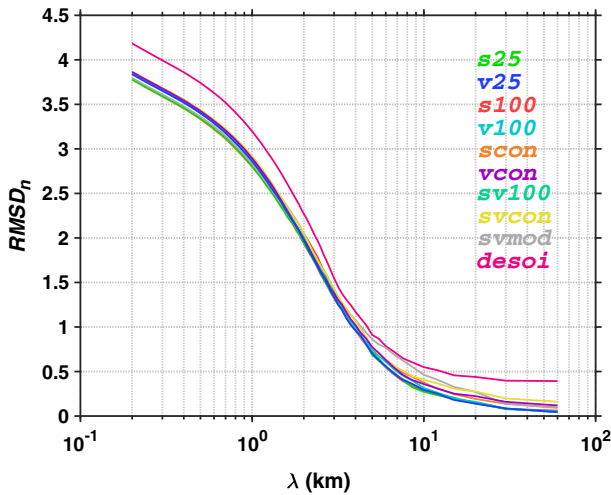


Fig. 11 Normalized $RMSD$ ($RMSD_n$) for the different cloud-cover deviations between the various sensitivity experiments and the *ref* simulation at 1200 UTC as a function of the cut-off wavelength

(soil moisture, land-use, orography, large-scale atmospheric conditions) in contrast to many existing studies using LES in an idealized set-up. The model domain encompasses a rural area in the Lower Rhine region (HD(CP)² investigation area) and is about $70 \text{ km} \times 70 \text{ km}$ in size. Here we find typical central European values for soil moisture and *LAI*. The region is characterized by flat to moderate orography. For the sensitivity tests 5 May 2013, a day within the HD(CP)² observing period, is chosen, a day, when the wind speed in the CBL is small (about 3 m s^{-1}) so that the surface fluxes can be assumed to dominate the boundary-layer turbulence. A high-resolution soil moisture dataset is generated by performing a stand-alone simulation with the TERRA-ML model, which is driven by COSMO-DE analyses and precipitation data from the DWD radar network. In this dataset the soil moisture in the uppermost 10 mm ranges from about 28–5% in the investigation area, with lower values in its northern and higher values in the southern part. In the reference simulation (*ref*), the soil- and vegetation parameters with the highest available resolution are used. For one set of sensitivity tests, the soil- and vegetation parameters are spatially-averaged over about $2.5 \text{ km} \times 2.5 \text{ km}$, $10 \text{ km} \times 10 \text{ km}$ and over the whole model domain. Spatial averaging leads to damping of the land-surface parameter amplitudes (e.g. the soil-moisture amplitude reduces from about 23% in the *ref* simulation, to 19% in the *s25* experiment, to 16% in the *s100* experiment). Additionally, one experiment with six modified soil moisture patches with $10 \text{ km} \times 10 \text{ km}$ in size is performed (*svmod* experiment). In these patches the soil moisture is increased and decreased so that the soil-moisture amplitude is about 20%, which is less than for the *ref* simulation but more than for the sensitivity experiment with the same resolution (*s100*). For all these simulations, the land-surface parameters have identical areal-mean values at initialization time. Finally, one experiment (*desoi*) is initiated with the soil moisture from COSMO-DE analysis data. For this experiment, the areal-mean soil moisture is about 21% compared to 19% in the other experiments.

As the initial areal means of the various land-surface parameters are equal for all simulations, except for the *desoi* experiment, the differences between the areal-mean energy balance components of these experiments are small. Consequently, the reduction in the land-surface parameter resolution does not modify the areal-mean potential temperature and specific

humidity in the mixed layer considerably. The largest deviations of the areal-mean CBL conditions are found for the *desoi* experiment, in which the CBL is colder, more humid and shallower. This is attributed to the higher soil moisture that led to higher/lower latent/sensible heat fluxes (lower Bowen ratio) compared to the other experiments. Moderate deviations in the CBL exist for the experiments with homogeneous land-surface conditions (e.g. *svcon* experiment). Spatial differences within the model domain are related to the magnitude of the land-surface anomaly. Considerable mesoscale secondary circulations are found when the soil moisture in some $10\text{ km} \times 10\text{ km}$ sized areas is modified by $\pm 30\%$ (*svmod* experiment) compared to the initial soil-moisture values in the *sv100* experiment. Convergence/divergence over and on the downwind side of patches with enhanced/reduced sensible heat flux develops. As the reduction of land-surface parameter resolution simultaneously reduces the magnitude of the anomalies, secondary circulations could not be observed in the other experiments.

Clouds develop in the upper part of the CBL in the morning hours in all simulations, with a cloud cover of about 11% reached around noon. Concerning the whole model domain, relative deviations of the areal-mean cloud cover between the sensitivity experiments and the *ref* simulation around noon are less than 10%. The only exception is the *desoi* experiment where about 30% more clouds are found than in the *ref* simulation. To assess the deviations of cloud cover on different scales, the *RMSD* value between the various sensitivity experiments and the *ref* simulation is calculated. The *RMSD*, normalized by the areal-mean cloud cover of the *ref* simulation, is designated as $RMSD_n$. To derive cloud-cover deviations for different spatial resolution, the cloud cover is low-pass filtered with different cut-off wavelengths. In general, $RMSD_n$ decreases continuously with an increase of the cut-off wavelength. For $\lambda < 1\text{ km}$, $RMSD_n > 3$, i.e. is greater than the areal-mean cloud cover itself. This is related to the stochastic nature of convection so that we can attribute the contribution of this effect to the $RMSD_n$ as “noise”. The strongest decrease can be found between $\lambda \approx 1\text{ km}$ and 5 km , and for the most “relevant” range of $\lambda > 5\text{ km}$, $RMSD_n < 1$. In this range, the cloud-cover deviations are produced by secondary circulations, i.e. they depend on the magnitude and extension of soil-moisture anomalies (as seen for the *svmod* experiment). Furthermore, the *desoi* experiment shows the largest $RMSD_n$ values at all wavelengths. This is because the cloud cover is generally higher in the whole model domain, implying that the absolute value of soil moisture has a significant influence on the cloud cover. The lowest $RMSD_n$ values can be found when the land-surface parameter resolution is only slightly lower (e.g. in the *s25* and *v25* experiment) than in the *ref* simulation. In that case, the $RMSD_n$ for $\lambda > 10\text{ km}$ is already < 0.25 .

Within this study we investigated the impact of land-surface parameter resolution on the cloud-topped boundary layer. This was motivated by the question as to whether we need these parameters on scales of a few hundred metres when applying LES? We found only a minor impact of resolution (land-surface parameter averaging) on cloud-cover differences when we compare it on scales of tenths of kilometres or larger. One reason is that averaging of high-resolution land-surface parameters, which gives an increase of the heterogeneity length scale, simultaneously reduces the amplitude of heterogeneity. Thereby, two effects mainly compensate each other concerning the impact on cloud cover. Increasing the amplitude of heterogeneity artificially causes secondary circulations, so that clear differences of cloud cover on the 10-km scale are present. In this case, the differences disappear when averaging over the whole model domain. In our investigation area, homogeneous land-surface parameters result in considerable surface-flux and boundary-layer differences on the half size of the domain, resulting in corresponding cloud cover differences. These differences disappear also for the whole-domain average. Considerable cloud-cover fraction differences for the whole domain only remain for the sensitivity experiment with an overall enhanced soil moisture. As

the results are obtained for a typical European rural landscape, where land-surface parameters do not differ considerably as for other climate zones or as often applied in idealistic model simulations, the conclusions are especially valid for such environments.

Acknowledgements This work was funded by the Federal Ministry of Education and Research in Germany (BMBF) as part of the research program ‘High Definition Clouds and Precipitation for Climate Prediction—HD(CP)²’ (FKZ: 01LK1205A). We thank the DWD-colleagues Jürgen Helmert for providing us with the version of the TERRA model that contains the use of the pedotransfer functions and Ulrich Blahak for his support concerning the LES version of the COSMO model. We thank the three anonymous reviewers for their constructive comments.

References

- Adler B, Kalthoff N, Gantner L (2011) Initiation of deep convection caused by land-surface inhomogeneities in West Africa: a modelled case study. *Meteorol Atmos Phys* 112:15–27
- Baldauf M, Seifert A, Förstner J, Majewski D, Raschendorfer M, Reinhardt T (2011) Operational convective-scale numerical weather prediction with the COSMO model: description and sensitivities. *Mon Weather Rev* 139(12):3887–3905
- Barthlott C, Hoose C (2015) Spatial and temporal variability of clouds and precipitation over Germany: multiscale simulations across the “gray zone”. *Atmos Chem Phys* 15:12361–12384
- Catalano F, Moeng CH (2010) Large-eddy simulation of the daytime boundary layer in an idealized valley using the weather research and forecasting numerical model. *Boundary-Layer Meteorol* 137(1):49–75. doi:10.1007/s10546-010-9518-8
- Caughey SJ (1982) Observed characteristics of the atmospheric boundary layer. In: Nieuwstadt FT, Van Dop H (eds) *Atmospheric turbulence and air pollution modelling*, Springer, Netherlands, pp 107–158
- Courault D, Drobinski P, Brunet Y, Lacarrere P, Talbot C (2007) Impact of surface heterogeneity on a buoyancy-driven convective boundary layer in light winds. *Boundary-Layer Meteorol* 124(3):383–403. doi:10.1007/s10546-007-9172-y
- Dixon NS, Parker DJ, Taylor CM, Garcia-Carreras L, Harris PP, Marsham JH, Polcher J, Woolley A (2013) The effect of background wind on mesoscale circulations above variable soil moisture in the Sahel. *Q J R Meteorol Soc* 139(673):1009–1024. doi:10.1002/qj.2012
- Fiori E, Parodi A, Siccardi F (2010) Turbulence closure parameterization and grid spacing effects in simulated supercell storms. *J Atmos Sci* 67(12):3870–3890. doi:10.1175/2010JAS3359.1
- Gantner L, Kalthoff N (2010) Sensitivity of a modelled life cycle of a mesoscale convective system to soil conditions over West Africa. *Q J R Meteorol Soc* 136(S1):471–482. doi:10.1002/qj.425
- Garcia-Carreras L, Parker DJ, Marsham JH (2011) What is the mechanism for the modification of convective cloud distributions by land surface-induced flows? *J Atmos Sci* 68(3):619–634
- Garratt JR (1994) *The atmospheric boundary layer*. Cambridge University Press, Cambridge, 316 pp
- Hanley KE, Plant RS, Stein THM, Hogan RJ, Nicol JC, Lean HW, Halliwell C, Clark PA (2015) Mixing-length controls on high-resolution simulations of convective storms. *Q J R Meteorol Soc* 141(686):272–284. doi:10.1002/qj.2356
- Heinze R, Dipankar A, Carbajal Henken C, Moseley C, Sourdeval O, Trömel S, Xie X, Adamidis P, Ament F, Baars H, Barthlott C, Behrendt A, Blahak U, Bley S, Brdar S, Brueck M, Crewell S, Deneke H, Di Girolamo P, Evaristo R, Fischer J, Frank C, Friederichs P, Göcke T, Gorges K, Hande L, Hanke M, Hansen A, Hege HC, Hoose C, Jahns T, Kalthoff N, Klocke D, Kneifel S, Knippertz P, Kuhn A, van Laar T, Macke A, Maurer V, Mayer B, Meyer CI, Muppa SK, Neggers RAJ, Orlandi E, Pantillon F, Pospichal B, Röber N, Scheck L, Seifert A, Seifert P, Senf F, Siligam P, Simmer C, Steinke S, Stevens B, Wapler K, Weniger M, Wulfmeyer V, Zängl G, Zhang D, Quaas J (2017) Large-eddy simulations over Germany using icon: a comprehensive evaluation. *Q J R Meteorol Soc* 143(702):69–100. doi:10.1002/qj.2947
- Heise E (2002) Die neue Modellkette des DWD I, 4: Parametrisierungen. *promet - Fortbildungszeitschrift des DWD* 27(3/4):130–141
- Herzog HJ, Schubert U, Vogel G, Fielder A, Kirchner R (2002a) LLM - the high-resolving nonhydrostatic simulation model in the DWD project LITFASS Part I, modelling technique and simulation method. *DWD Forschung und Entwicklung: Arbeitsergebnisse* 67:75 S
- Herzog HJ, Vogel G, Schubert U (2002b) LLM: a nonhydrostatic model applied to high-resolving simulations of turbulent fluxes over heterogeneous terrain. *Theor Appl Climatol* 73(1–2):67–86. doi:10.1007/s00704-002-0694-4

- Honnert R, Masson V, Couvreux F (2011) A diagnostic for evaluating the representation of turbulence in atmospheric models at the kilometric scale. *J Atmos Sci* 68:31123131. doi:[10.1175/JAS-D-11-061.1](https://doi.org/10.1175/JAS-D-11-061.1)
- Hozumi K, Harimaya T, Magono C (1982) The size distribution of cumulus clouds as a function of cloud amount. *J Meteorol Soc Jpn* 60:691–699
- Huang HY, Margulis SA (2013) Impact of soil moisture heterogeneity length scale and gradients on daytime coupled land-cloudy boundary layer interactions. *Hydrol Process* 27(14):1988–2003
- Khodayar S, Kalthoff N, Schädler G (2013) The impact of soil moisture variability on seasonal convective precipitation simulations: Part 1: validation, feedbacks, and realistic initialisation. *Meteorol Z* 22(4):489–505
- Kohler M, Kalthoff N, Kottmeier C (2010) The impact of soil moisture modifications on CBL characteristics in West Africa: A case study from the AMMA campaign. *Q J R Meteorol Soc* 136(S1):442–455. doi:[10.1002/qj.430](https://doi.org/10.1002/qj.430)
- Kohler M, Schädler G, Gantner L, Kalthoff N, Königer F, Kottmeier C (2012) Validation of two SVAT models for different periods during the West African monsoon. *Meteorol Z* 21(5):509–524
- Langhans W, Schmidli J, Schär C (2012) Bulk convergence of cloud-resolving simulations of moist convection over complex terrain. *J Atmos Sci* 69(7):2207–2228
- Larson VE, Schanen DP, Wang M, Ovchinnikov M, Ghan S (2012) PDF parameterization of boundary layer clouds in models with horizontal grid spacings from 2 to 16 km. *Mon Weather Rev* 140(1):285–306
- Lenschow DH, Wyngaard JC, Pennell WT (1980) Mean-field and second-moment budgets in a baroclinic, convective boundary layer. *J Atmos Sci* 37(6):1313–1326
- Lenschow DH, Lothon M, Mayor SD, Sullivan PP, Canut G (2012) A comparison of higher-order vertical velocity moments in the convective boundary layer from lidar with in situ measurements and large-eddy simulation. *Boundary-Layer Meteorol* 143(1):107–123
- Lohou F, Patton EG (2014) Surface energy balance and buoyancy response to shallow cumulus shading. *J Atmos Sci* 71(2):665–682
- Macke A, Seifert P, Baars H, Beekmans C, Behrendt A, Bohn B, Bühl J, Crewell S, Damian T, Deneke H, Düsing S, Foth A, Girolamo PD, Hammann E, Heinze R, Hirsikko A, Kalisch J, Kalthoff N, Kinne S, Kohler M, Löhnert U, Madhavan BL, Maurer V, Muppa SK, Schween J, Serikov I, Siebert H, Simmer C, Späth F, Steinke S, Träumner K, Wehner B, Wieser A, Wulfmeyer V, Xie X (2017) The HD(CP)² observational prototype experiment (HOPE) - an overview. *Atmos Chem Phys* 17(7):4887–4914. doi:[10.5194/acp-17-4887-2017](https://doi.org/10.5194/acp-17-4887-2017)
- Maronga B, Raasch S (2013) Large-eddy simulations of surface heterogeneity effects on the convective boundary layer during the LITFASS-2003 experiment. *Boundary-Layer Meteorol* 146(1):17–44. doi:[10.1007/s10546-012-9748-z](https://doi.org/10.1007/s10546-012-9748-z)
- Mason P (1994) Large-eddy simulation: a critical review of the technique. *Q J R Meteorol Soc* 120:1–26
- Mason P, Brown A (1999) Large-eddy simulation: On subgrid models and filter operations in large eddy simulations. *J Atmos Sci* 56:2101–2114
- Maurer V, Kalthoff N, Wieser A, Kohler M, Mauder M (2016) Observed spatial variability of boundary-layer turbulence over flat, heterogeneous terrain. *Atmos Chem Phys* 16:1377–1400
- Nachtergaele F, van Velthuizen H, Verelst L, Wiberg D (2012) Harmonized World Soil Database, Version 1.2. Technical Report
- Ookouchi Y, Segal M, Kessler R, Pielke R (1984) Evaluation of soil moisture effects on the generation and modification of mesoscale circulations. *Mon Weather Rev* 112(11):2281–2292
- Petch JC, Brown AR, Gray MEB (2002) The impact of horizontal resolution on the simulations of convective development over land. *Q J R Meteorol Soc* 128(584):2031–2044. doi:[10.1256/003590002320603511](https://doi.org/10.1256/003590002320603511)
- Pielke RA (2001) Influence of the spatial distribution of vegetation and soils on the prediction of cumulus convective rainfall. *Rev Geophys* 39(2):151–177. doi:[10.1029/1999RG000072](https://doi.org/10.1029/1999RG000072)
- Plank VG (1969) The size distribution of cumulus clouds in representative florida populations. *J Appl Meteorol* 8(1):46–67
- Raasch S, Harbusch G (2001) An analysis of secondary circulations and their effects caused by small-scale surface inhomogeneities using large-eddy simulation. *Boundary-Layer Meteorol* 101(1):31–59. doi:[10.1023/A:1019297504109](https://doi.org/10.1023/A:1019297504109)
- Ricard D, Lac C, Riette S, Legrand R, Mary A (2013) Kinetic energy spectra characteristics of two convection-permitting limited-area models AROME and Meso-NH. *Q J R Meteorol Soc* 139(674):1327–1341. doi:[10.1002/qj.2025](https://doi.org/10.1002/qj.2025)
- Rieck M, Hohenegger C, van Heerwaarden CC (2014) The influence of land surface heterogeneities on cloud size development. *Mon Weather Rev* 142(10):3830–3846
- Rieck M, Hohenegger C, Gentine P (2015) The effect of moist convection on thermally induced mesoscale circulations. *Q J R Meteorol Soc* 141:2418–2428. doi:[10.1002/qj.2532](https://doi.org/10.1002/qj.2532)

- Ritter B, Geleyn JF (1992) A comprehensive radiation scheme for numerical weather prediction models with potential applications in climate simulations. *Mon Weather Rev* 120(2):303–325. doi:[10.1175/1520-0493\(1992\)120<0303:ACRSFN>2.0.CO;2](https://doi.org/10.1175/1520-0493(1992)120<0303:ACRSFN>2.0.CO;2)
- Schättler U, Doms G, Schraff C (2014) A description of the nonhydrostatic regional COSMO-model, Part VII: User's Guide. Technical Report, Deutscher Wetterdienst, Offenbach, Germany
- Schwendike J, Kalthoff N, Kohler M (2010) The impact of mesoscale convective systems on the surface and boundary-layer structure in West Africa: Case-studies from the AMMA campaign 2006. *Q J R Meteorol Soc* 136(648):566–582. doi:[10.1002/qj.599](https://doi.org/10.1002/qj.599)
- Segal M, Arritt R (1992) Nonclassical mesoscale circulations caused by surface sensible heat-flux gradients. *Bull Am Meteorol Soc* 73(10):1593–1604
- Shen S, Leclerc MY (1995) How large must surface inhomogeneities be before they influence the convective boundary layer structure? A case study. *Q J R Meteorol Soc* 121(526):1209–1228. doi:[10.1002/qj.49712152603](https://doi.org/10.1002/qj.49712152603)
- Shin HH, Hong SY (2013) Analysis of resolved and parameterized vertical transports in convective boundary layers at gray-zone resolutions. *J Atmos Sci* 70(10):3248–3261
- Shuttleworth WJ (1991) Evaporation models in hydrology. In: Schmugge TJ, André J-C (eds) *Land surface evaporation*. Springer, New York, pp 93–120
- Siebert J, Sievers U, Zdankowski W (1992) A one-dimensional simulation of the interaction between land surface processes and the atmosphere. *Boundary-Layer Meteorol* 59(1–2):1–34. doi:[10.1007/BF00120684](https://doi.org/10.1007/BF00120684)
- Smiatke G, Helmert J, Gerstner EM (2016) Impact of land use and soil data specifications on COSMO-CLM simulations in the CORDEX-MED area. *Meteorol Z* 25(2):215–230. doi:[10.1127/metz/2015/0594](https://doi.org/10.1127/metz/2015/0594)
- Stein T, Hogan RJ, Clark PA, Halliwell CE, Hanley KE, Lean HW, Nicol JC, Plant RS (2015) The DYMECS project: a statistical approach for the evaluation of convective storms in high-resolution NWP models. *Bull Am Meteorol Soc* 96:939–951. doi:[10.1175/BAMS-D-13-00279.1](https://doi.org/10.1175/BAMS-D-13-00279.1)
- Sun WY, Bosilovich M (1996) Planetary boundary layer and surface layer sensitivity to land surface parameters. *Boundary-Layer Meteorol* 77(3–4):353–378. doi:[10.1007/BF00123532](https://doi.org/10.1007/BF00123532)
- Talbot C, Bou-Zeid E, Smith J (2012) Nested mesoscale large-eddy simulations with WRF: performance in real test cases. *J Hydrometeorol* 13(5):1421–1441
- Taylor CM, Parker DJ, Harris PP (2007) An observational case study of mesoscale atmospheric circulations induced by soil moisture. *Geophys Res Lett* 34(L15):801. doi:[10.1029/2007GL030572](https://doi.org/10.1029/2007GL030572)
- van Genuchten MT (1980) A closed-form equation for predicting the hydraulic conductivity of unsaturated soils. *J Appl Meteorol* 54(1):189–206. doi:[10.1175/JAMC-D-14-0140.1](https://doi.org/10.1175/JAMC-D-14-0140.1)
- van Heerwaarden CC, Mellado JP, De Lozar A (2014) Scaling laws for the heterogeneously heated free convective boundary layer. *J Atmos Sci* 71(11):3975–4000. doi:[10.1175/JAS-D-13-0383.1](https://doi.org/10.1175/JAS-D-13-0383.1)
- Wetzel PJ, Chang JT (1988) Evapotranspiration from nonuniform surfaces: a first approach for short-term numerical weather prediction. *Mon Weather Rev* 116(3):600–621
- Wösten JHM, Lilly A, Nemes A, Le Ba C (1999) Development and use of a database of hydraulic properties of European soils. *Geoderma* 90:169–185